J. Phys.: Condens. Matter **22** (2010) 205504 (7pp) doi:10.1088/0953-8984/22/20/205504

Atomic and electronic structures of amorphous $Ge_2Sb_2Te_5$; melt-quenched versus ideal glasses

E Cho[1], J Im[2], C Park[2], W J Son[1], D H Kim[3], H Horii[3], J Ihm[2] and S Han[1]

[1] Department of Materials Science and Engineering, Seoul National University, Seoul 151-744, Korea
[2] Department of Physics and Astronomy, Seoul National University, Seoul 143-747, Korea
[3] Process Development Team, Semiconductor R&D Center, Samsung Electronics, Hwasung 445-701, Korea

E-mail: hansw@snu.ac.kr

Received 10 February 2010, in final form 1 April 2010
Published 30 April 2010
Online at stacks.iop.org/JPhysCM/22/205504

Abstract

To investigate an amorphous structure of $Ge_2Sb_2Te_5$ that satisfies the 8-N rule (so-called 'ideal glass'), we perform alternative melt-quench simulations on $Si_2As_2Se_5$ and replace atoms in the final structure with Ge–Sb–Te. The resulting structures have salient features of the 8-N rule such as the tetrahedral configuration for all Ge atoms and the localized Te lone pairs at the valence top. In addition, the average Ge–Te and Sb–Te distances are in good agreement with experiment. The energetic stability of the ideal glass supports the existence of this amorphous structure that is distinct from the melt-quenched glass. From the analysis of electronic structures and optical dielectric constants, it is concluded that the electronic character of the melt-quenched amorphous $Ge_2Sb_2Te_5$ lies in between the resonant p-bonding of the crystalline phase and the covalent bonding of the ideal glass.

(Some figures in this article are in colour only in the electronic version)

1. Introduction

The distinct physical properties between amorphous and crystalline phases have enabled chalcogenide compounds to be a material of choice for various technological applications, in particular high-density non-volatile memories [1]. For example, the rewritable optical storage media comprising chalcogenides exploit a large change in the reflectivity upon amorphization. The phase-change memory, a leading contender for the next-generation non-volatile random-access memories, is based on the conductivity contrast between the two phases. In both applications, the phase change can be achieved on a nanosecond scale via laser or current pulses, allowing for a fast data transfer.

Understanding of the phase-change phenomena in chalcogenides is not only fundamentally intriguing but also critical to overcome various technical barriers. The first step towards this goal would be to establish the atomic and electronic structures of crystalline and amorphous phases at the microscopic level. For example, $(GeTe)_n(Sb_2Te_3)_m$ or GST, a representative phase-change pseudobinary alloy, is known to crystallize into a rocksalt structure where Te atoms fully occupy one sublattice site while Ge and Sb atoms sit on the other sublattice site randomly with a certain fraction of the vacancy to satisfy the given stoichiometry [2]. In contrast, the amorphous structure of GST has not been fully clarified. The recent spectroscopic studies using extended x-ray absorption fine structure (EXAFS) consistently show that the bonding nature in the amorphous GST is markedly different from that in the crystalline state [3, 4]. For instance, the bond lengths are significantly reduced, which can be contrasted to the fact that the specific volume of GST expands upon amorphization. Refinement using the reverse Monte Carlo (RMC) method [5] or the bond constraint theory [4] also showed that the coordination numbers are greatly reduced in the amorphous structure. To be specific, in [5], the

coordination numbers for Ge, Sb and Te atoms in $Ge_2Sb_2Te_5$ were estimated to be 3.85, 3.12 and 1.99, respectively, while they are 3.9, 2.8 and 2.4 in [4]. In addition, the spectroscopic data was best fitted when all Ge atoms were assumed to be in the tetrahedral configuration, implying that Ge atoms form sp^3 bonds with neighboring atoms [3]. Therefore, the local coordination numbers in the amorphous GST broadly satisfy the '8-*N* rule' [6]. Here, the 8-*N* rule indicates that the coordination number for an atom is 8-*N* if *N* is the number of valence electrons. According to this rule, Ge, Sb and Te atoms are four-, three-and twofold-coordinated, respectively, since the number of valence electrons are 4 (Ge), 5 (Sb) and 6 (Te). An amorphous structure with strict adherence to the 8-*N* rule is called an 'ideal glass' [7], meaning that the covalent needs of constituent atoms are satisfied without exception. Therefore, it can be concluded that the amorphous GST in experiments resembles an ideal glass in many respects.

Theoretically, a series of first-principles molecular dynamics (MD) simulations [8–14] have been performed to obtain amorphous structures directly by mimicking the melt-quench process. However, the simulation consistently produced amorphous structures with a local ordering at variance with experiment. Most significantly, a large fraction of Ge atoms in the simulation are in the octahedral configuration, in contrast to the purely tetrahedral Ge sites shown by experiment (see above). This leads to a bond length in the Ge–Te pair that is longer than the experimental measurement by ∼0.2 Å. In addition, the coordination numbers also deviate from the experimental observations and those for Sb and Te atoms are significantly overestimated. For example, in [8], the coordination numbers for Sb and Te were computed to be 3.7 and 2.9, respectively. (We note that some progress has been made by combining the experiment and first-principles calculations [11].) Therefore, the amorphous model emerging from the MD simulations is clearly at variance with the experiment. To address the discrepancy between theory and experiment, it is critical to obtain an amorphous structure with local atomic arrangements close to the ideal glass and investigate its atomic and electronic structures. In this paper, we achieve this by making use of the corresponding structure of Si–As–Se compounds. The obtained amorphous structure is in good agreement with experiment. The structural and electronic properties will be compared with the crystalline phase as well as the melt-quenched glass.

2. Computational methods

We employ first-principles methods based on the density functional theory throughout this work. Among various GST compounds, we choose $Ge_2Sb_2Te_5$ which has been receiving particular attention recently as the material satisfies various technical requirements for PRAM such as the rapid phase change and good stability [15]. We use the Vienna *ab initio* simulation package (VASP) [16] for MD simulations and the electronic structure calculations. The projector-augmented-wave (PAW) pseudopotentials [17] are used to describe electron–ion interactions. For the exchange–correlation energies between electrons, the generalized gradient approximation based on the Perdew–Burke–Ernzerhof (PBE) functional [18] is employed. The energy cutoff for the plane-wave basis expansion is chosen to be 250 eV. For the *k*-point sampling, we choose a single point of (1/4, 1/4, 1/4), the so-called Baldereschi point [19], for MD simulations. From several tests, it is found that the Γ-point alone is not enough to ensure the full convergence in total energy and forces for the supercell size used in the present work. For the ensuing structural relaxation and analysis on the electronic structure, $2 \times 2 \times 2$ *k*-point grids are used. The temperature during the cooling process is controlled at every MD step (with an interval of 2–3 fs) by rescaling the atomic velocities. The density of states is smeared by Gaussian functions with a width of 0.05 eV. The atomic positions are relaxed until the Hellmann–Feynman force on each atom is reduced to within 0.03 eV $Å^{-1}$. In order to examine the functional dependence, the final structures are fully relaxed again within the local density approximation [20]. In addition, the hybrid functionals based on PBE0 [21] and the Heyd–Scuseria–Ernzerhof (HSE) [22] framework are also tested on selected configurations. In the HSE scheme, the screening parameter to truncate the long-range Fock potential is set to 0.2 $Å^{-1}$. In [12], it was noted that the energy gap of the crystalline phase is well described by the HSE functional. In calculating dielectric constants and Born effective charges, we employ the computational package of Quantum-ESPRESSO [23]. For statistical sampling, five configurations with different initial configurations are considered for each structure.

3. Results and discussions

We first obtain the amorphous structure through the melt-quench process similar to the previous literature. The initial crystalline phase includes 72 atoms within the orthorhombic supercell and the cation sites are randomly occupied with Ge or Sb atoms (see figure 1(a)). The supercell is expanded by 6.7% to match the amorphous volume and is melted for 12 picoseconds (ps) at 2000 K to erase the crystalline information. The liquid is then cooled to 1000 K and melted for 30 ps additionally. The liquid structure is subsequently quenched from 1000 to 300 K with a cooling rate of -15 K ps^{-1}. The final structure is fully relaxed at 0 K including lattice parameters. One of the obtained melt-quenched structures is shown in figure 1(b).

The resulting structure for the melt-quenched glass is consistent with previous MD studies. In table 1, the density and energy are compared between crystalline and amorphous phases. As the volume expands upon amorphization, the density decreases by 7.3% (3% in LDA), in reasonable agreement with the experimental value of 6.4% [24]. On the other hand, the total energy of the amorphous structure is higher than for the crystalline phase by 96 meV/atom (119 meV/atom for LDA), in comparison with 65 meV/atom in [13]. The discrepancy can be attributed to the fact that the simulation volume in [13] was fixed to a value between those for the crystalline and amorphous phases.

The coordination number of each atom is obtained by integrating the partial radial distribution functions (RDFs) for

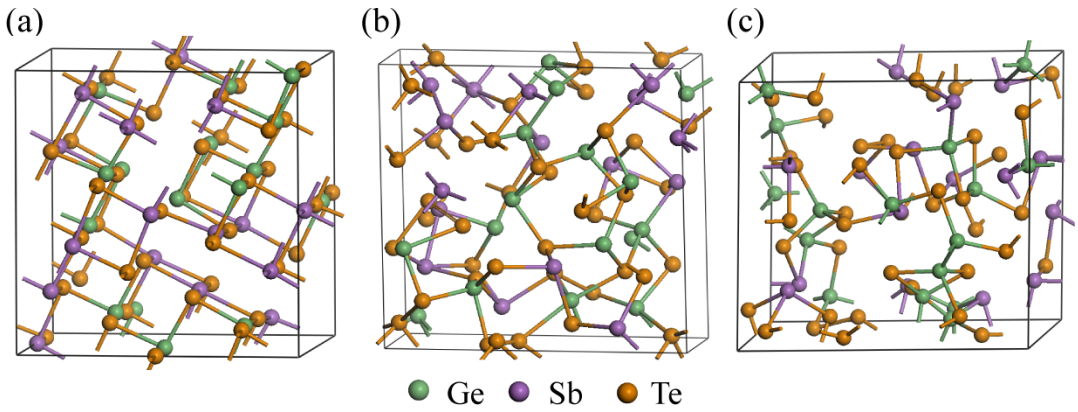

Figure 1. The representative structures of $Ge_2Sb_2Te_5$ including 72 atoms. (a) The crystalline phase, (b) the melt-quenched glass obtained from a melt-quench process and (c) the ideal glass obtained from a melt-quench simulation on $Si_2As_2Se_5$.

Table 1. The density and energy for crystalline and amorphous $Ge_2Sb_2Te_5$. GGA and LDA values are averaged over five configurations and the standard deviations are noted within the parentheses. The results from the hybrid functional (PBE0 and HSE) are for the configurations in figure 1.

	Density (atoms Å^{-3})			Energy (meV/atom)			
	GGA	LDA	Exp.[a]	GGA	LDA	PBE0	HSE
Crystal	0.0313 (±0.0001)	0.0344 (±0.0001)	0.0330	0 (±3.0)	0 (±3.4)	0	0
Melt-quench	0.0290 (±0.0007)	0.0334 (±0.0004)	0.0309	96 (±6.6)	119 (±7.9)	87	89
Ideal glass	0.0268 (±0.0003)	0.0319 (±0.0005)		117 (±7.1)	154 (±10)	91	93

[a] Reference [24].

Table 2. The coordination numbers, bond lengths and the number of fourfold rings for crystalline and amorphous structures of $Ge_2Sb_2Te_5$. The values for the crystal, melt-quenched and ideal glass structures are averaged over five configurations and the standard deviations are noted within the parentheses. IG1 and IG2 indicate the structures obtained after performing an additional heating cycle at 800 and 1000 K on the ideal glass, respectively.

	Coordination number			Bond length (Å)		
	Ge	Sb	Te	Ge–Te	Sb–Te	Fourfold rings
Crystal	6.0	6.0	4.8	2.87 (±0.04)	2.95 (±0.01)	120
Melt-quench	3.8 (±0.10)	3.3 (±0.08)	2.6 (±0.07)	2.80 (±0.03)	2.90 (±0.01)	21 (±3.9)
Melt-quench (Other theory)[a]	4.2	3.7	2.9	2.78	2.93	
Ideal glass	4.0 (±0.05)	3.0 (±0.10)	2.1 (±0.07)	2.65 (±0.01)	2.88 (±0.01)	7 (±4.0)
IG1 (800 K)	3.6	3.2	2.4	2.75	2.86	14
IG2 (1000 K)	3.5	3.3	2.4	2.73	2.87	10
Experiment[b]	3.85–3.90	2.80–3.12	1.99–2.40	2.60–2.63	2.82–2.85	

[a] Reference [8]. [b] Reference [3–5].

each atomic species from the origin up to the first dip position, which turns out to be 3.2 Å for all atoms. The results are summarized in table 2 and it can be seen that the data show significant deviations from the 8-*N* rule. The total RDF in figure 2(a) also indicates that the first peak is substantially shifted outwards in comparison to the experimental data [25]. (It was found in [13] that the agreement could be improved by changing the pseudopotential type.) The bond length of the atomic pair is obtained by reading the position of the first peak in the corresponding partial RDF. For example, in the case of the Ge–Te pair in figure 2(b), the bond length for the melt-quenched glass is 2.82 Å which is significantly larger than the experimental value of 2.60–2.63 Å [3–5].

To obtain an ideal glass structure for $Ge_2Sb_2Te_5$, we perform a similar melt-quench simulation on the hypothetical $Si_2As_2Se_5$ compound with the rocksalt structure. This was motivated by the observation that, as one goes up the Periodic Table, the smaller difference between s- and p-orbital radii enhances the sp hybridization, resulting in a more covalent bonding character [26, 27]. Since the 8-*N* rule

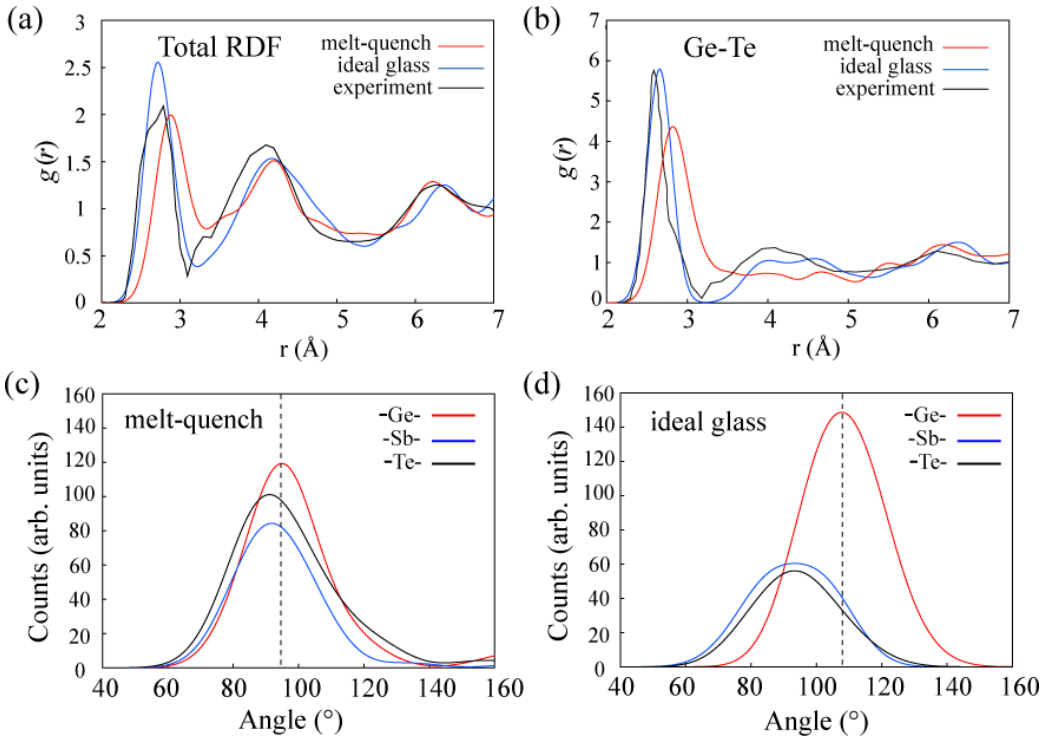

Figure 2. The structural properties of amorphous $Ge_2Sb_2Te_5$. (a) The total RDF. The experimental data was reconstructed from [25]. (b) The partial RDF of Ge–Te. The experimental data is from RMC results in [5]. (c) and (d) show the angular distributions of chemical bonds around Ge, Sb and Te atoms for the melt-quenched and ideal glasses, respectively. The theoretical distributions are smeared with Gaussian functions of 0.10 Å or 8.0° width. The dashed lines denote the peak position in the distribution for Ge.

is the manifestation of the covalent bond, it is likely that the amorphous $Si_2As_2Se_5$ would better satisfy the 8-*N* rule. Indeed, the amorphous structure of $Si_2As_2Se_5$ obtained by following a temperature protocol similar to the above shows that the coordination number obeys the 8-*N* rule precisely[4]. The elements are then replaced with Ge–Sb–Te and the structure is fully relaxed including the cell shape and volume. The final amorphous $Ge_2Sb_2Te_5$, which we call the ideal glass hereafter, also closely satisfy the 8-*N* rule, as will be shown in the following analysis. A representative configuration of the ideal glass is shown in figure 1(c).

In table 2, the calculated coordination numbers of the ideal glass are 4.0 (Ge), 3.0 (Sb) and 2.1 (Te), strictly obeying the 8-*N* rule. The atom-resolved coordination numbers for Ge are 2.94 (Ge–Te), 0.16 (Ge–Ge) and 0.88 (Ge–Sb). In comparison, the corresponding RMC results are 2.45, 0.79 and 0.60, respectively [5]. Even though Ge–Ge bonds are less frequent in the current simulation than in the RMC data, the percentage of cationic homopolar bonds (Ge–Ge or Ge–Sb) is in reasonable agreement. The discrepancy could be ascribed to the different chemistry between Si–As–Se and Ge–Sb–Te alloys. On the other hand, the partial coordination number for Te–Te bonds is only 0.17, meaning that the anion–anion homopolar bond is energetically unstable. (This pair was completely neglected in RMC [5].) In the last column of table 2, we also compare the numbers of fourfold rings which are building blocks in the crystalline GST. The fourfold rings almost disappear in the ideal glass, indicating that the ideal glass is furthest from the crystalline structure in terms of local order.

It is worth mentioning that the coordination numbers in the amorphous structure are not clearly defined and can vary depending on the cutoff radii. However, there are two hallmark features that should be present in the amorphous GST that obeys the 8-*N* rule [14]. First, if Ge atoms are fourfold-coordinated, the tetrahedral configuration should be favored energetically. Second, as the Te atoms are twofold-coordinated, the localized Te lone pairs should appear at the valence top [28]. As will be shown below, the ideal glass obtained in the present study has these features, and therefore can be regarded as truly satisfying the 8-*N* rule.

In figures 2(a) and (b), RDFs are compared between the crystalline phase, the melt-quenched glass and the ideal glass. Even though there are some disparities in the total RDF between theory and experiment, the position of the first peak is much better reproduced in the ideal glass (see figure 2(a)). The partial RDF for the Ge–Te pair in figure 2(b) indicates that the Ge–Te bonding distance is 2.64 Å, noticeably shorter than for the melt-quenched structure (2.82 Å) as well as for the crystalline phase (2.84 Å). This value is close to the EXAFS measurements of 2.60–2.63 Å [3–5]. Similarly, Sb–Te distances are 2.92 and 2.89 Å for the melt-quenched and ideal glasses, respectively, while the experiments give 2.82–2.85 Å [3–5]. Again, the bond length is better described in the ideal glass.

[4] The melting point is set to 2000 K but the cooling rate is accelerated to be -75 K ps^{-1}. A test simulation with a slower cooling rate of -15 K ps^{-1} did not produce any meaningful differences in the final structure.

The angular distribution functions (ADFs) around Ge, Sb and Te atoms are shown in figures 2(c) and (d) for the melt-quenched and ideal glasses, respectively. For the ideal glass, the ADF around the Ge atom is peaked at 106° and this is close to the nominal tetrahedral bond angle of 109.5°. This indicates that most Ge atoms are tetrahedrally coordinated, which is consistent with the RMC results [5]. On the other hand, the maximum of ADF around Ge is located at 95° for the melt-quenched glass, meaning that octahedral Ge atoms are more populated than tetrahedral ones. Although the local structure of the simulated ideal glass matches very well with the experiment, the density reduction is overestimated by a factor of 2 (see table 1). This can be ascribed to the small supercell size which affects the covalent network of the ideal glass more seriously than the melt-quenched glass. (It is noted that LDA values are in better agreement with the experiment.)

In table 1, the energetic stability is compared among crystalline and amorphous structures. As mentioned above, the total energy is averaged over five configurations for each structure. It is found that the energetic stability is in the sequence of crystal > melt-quenched glass > ideal glass in both GGA and LDA. The higher energy of the ideal glass against the melt-quenched structure may explain why the ideal glass was not observed in MD simulations. However, the energy difference between two amorphous structures is rather small (∼20 meV/atom). It should be noted that the different chemistry between Si–As–Sb and Ge–Sb–Te may have increased the total energy of the ideal glass. In addition, the covalent nature of the ideal glass implies that the structure could be more sensitive to the supercell size as noted above. Considering these unfavorable conditions in constructing the ideal glass in the present work, one cannot exclude a possibility that the optimized ideal glass is energetically more stable than the melt-quenched glass. Then, it would be meaningful to ask why none of the melt-quench simulations produced an ideal glass. One plausible explanation could be based on the lattice contribution to the free energy; because of the covalent bonding character, it is anticipated that the phonon modes in the ideal glass are hardened in comparison with those in the melt-quenched glass. For example, in [12], the high-frequency phonon modes around 200 cm^{-1} were found in the melt-quenched glass and they were assigned to the modes localized on tetrahedral Ge atoms. The free energy of a simple harmonic oscillator with a frequency of ω is given at temperature T as $\hbar\omega/2 + k_B T \ln(1 - \exp(-\hbar\omega/k_B T))$, where $\hbar$ is the Planck constant and k_B is the Boltzmann constant. Supposing that phonon modes are hardened from 100 to 200 cm^{-1}, the free energy increases by 20–30 meV/mode in the temperature range of 400–600 K which corresponds to the glass transition temperatures of $Ge_2Sb_2Te_5$ [29]. This amount of an energy increase is comparable to the difference in the total energy per atom between melt-quenched and ideal glasses. Therefore, the vibrational part of the free energy can play a significant role in destabilizing the ideal glass as the material is cooled down from the liquid phase.

In the last column in table 1, the total energies calculated with the hybrid functional are compared between the three structures in figure 1. Interestingly, the energy of the ideal glass is much lowered and very close to the values for the melt-quenched glass. The unphysical self-interaction in the Te lone pairs (see below) might have been cured by the exact exchange interaction in the hybrid functional. Therefore, if one can carry out melt-quench simulations on $Ge_2Sb_2Te_5$ using the hybrid functional, a structure close to the ideal glass might be obtained. However, due to the sheer cost in calculating the Fock potential, the computation is not viable within our computational capacity.

In order to investigate the stability at finite temperatures, we anneal the ideal glass at 300 and 500 K for 20 ps. It is found that the structure remains stable at 300 K and the overall bonding configurations are maintained. However, at 500 K, the local coordination slightly changes and the octahedral Ge atoms begin to appear, implying that the system gradually evolves towards a melt-quenched structure that is energetically more stable. This might be partly driven by the lattice free energy described above.

To further study the stability of the ideal glass, we carry out a full heating cycle at higher temperatures as follows; we first start with the most stable ideal glass found in our simulations and heat the structure at 800 and 1000 K for 20 ps and cooled it down to 300 K with a cooling rate of -15 K ps^{-1}. We call these two structures IG1 and IG2. After full relaxation, the energies of IG1 and IG2 are 89 and 95 meV/atom higher than for the crystalline phase. As can be seen in table 1, these are similar to the values for melt-quenched structures. In fact, IG1 is very close to the most stable melt-quenched glass obtained in the present study (87 meV/atom). The structural analyses on IG1 and IG2 are provided in table 2. Interestingly, IG1 and IG2 are in between the melt-quenched and ideal glasses in many respects except for the coordination numbers for Ge. These results support again a possibility of a low-energy glass structure that is distinct from the melt-quenched glass.

Next, we examine the electronic structure of the crystalline and amorphous $Ge_2Sb_2Te_5$. In figures 3(a)–(c), the partial density of states (PDOS) is shown for the structures in figure 1. All three structures have energy gaps around 0.2–0.3 eV. Near the Fermi level, significant differences are observed in PDOS between the three structures, particularly for Ge atoms; while the partial contribution of Ge atoms to the valence and conduction edges are dominated by 4s and 4p characters, respectively, the relative weight is reversed in the ideal glass. A similar observation can be found for Sb atoms near the valence edge. The PDOS of the crystalline Ge in the diamond structure, which represents the covalent limit, shows that the valence top is mostly contributed by 4p orbitals. Therefore, the reduction of the s character of Ge atoms near the Fermi level can be regarded as an indication that the covalent bonding character was developed. From the relative contributions among orbitals, it is observed that the electronic character of the melt-quenched glass lies in between those of the crystalline phase and ideal glass. In figure 3(c), localized peaks are noticeable at the valence top (dashed circle). The spatial distribution in figure 3(d) indicates that they are derived from the lone pair of Te atoms, with the 5p orbital pointing normal to the plane formed by two Te–(Ge, Sb) bonds.

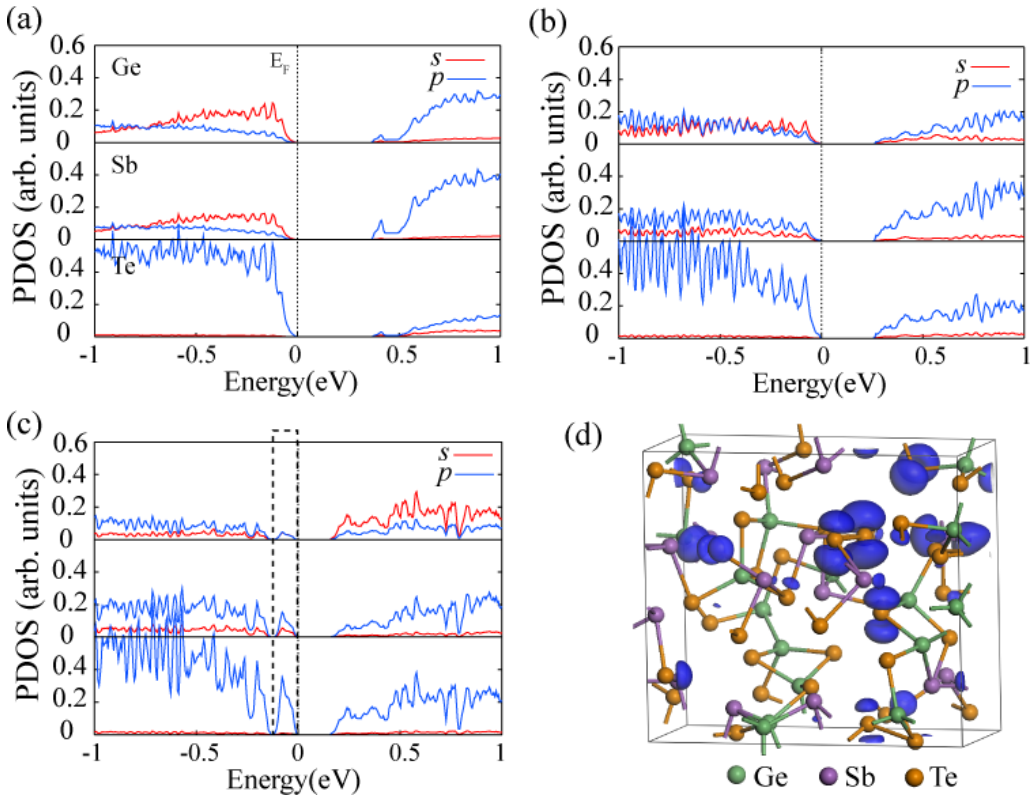

Figure 3. The projected density of states (PDOS) for (a) the crystalline phase, (b) the melt-quenched glass and (c) the ideal glass. The Fermi level is set to zero. (d) The isosurface plot of the sum of valence top states in the ideal glass (dashed box in (c)).

The gradual change of the electronic character along the crystalline phase, the melt-quenched glass and the ideal glass is further confirmed in the dielectric response as shown in table 3. The optical dielectric constants (ε^{∞}) and the averaged Born effective charges (Z^*) are calculated based on density functional perturbation theory [30] implemented within PWSCF [23]. Z^* is evaluated by taking the average of the trace of the Born charge tensor divided by three. For comparison, the static charges from Bader analysis [31] are also evaluated in table 3. The experimental values of ε^{∞} are 33.3 and 16.0 for crystalline and amorphous phases, respectively [32]. The overestimation of ε^{∞} for the crystalline phase might originate from the underestimation of the energy gap in the density functional calculations [12]. In [32], the large ε^{∞} for the crystalline phase was attributed to the resonant p-bonding network which enhances the atomic polarizability. In the ideal glass, the symmetry condition necessary for the resonant bonding is broken as the sp hybridization makes the bonding more directional. This results in the decreased ε^{∞} for the ideal glass. In table 3, the monotonic decrease of the dielectric constant and the magnitude of dynamic and static charges are noticeable. This again indicates that the bonding character changes gradually from the resonant bonding character in the crystalline phase to a more covalent bonding in the ideal glass. We note that similar trends in the optical response and effective charges were found as the local distortions were introduced in the GeTe crystal [33].

Table 3. Optical dielectric constants (ε^{∞}), averaged Born effective charges and averaged static charges from Bader analysis for crystalline and amorphous $Ge_2Sb_2Te_5$.

		Born charges ($\|e\|$)			Static charges ($\|e\|$)		
	ε^{∞}	Ge	Sb	Te	Ge	Sb	Te
Crystal	50.5	5.9	7.8	−5.5	0.44	0.61	−0.42
Melt-quench	34.3	2.9	3.3	−2.4	0.44	0.53	−0.39
Ideal glass	21.4	1.9	2.3	−1.6	0.37	0.44	−0.32

4. Conclusion

We have successfully obtained amorphous $Ge_2Sb_2Te_5$ structures that closely obey the 8-N rule. The bond lengths between atomic pairs are in good agreement with experiment. In addition, the resulting structures have salient features of the 8-N rule such as the tetrahedral configurations for all Ge atoms and the localized Te lone pairs at the valence top. The analysis on the energetic stability implies that either the melt-quenched glass or the ideal glass can be formed for $Ge_2Sb_2Te_5$, depending on the amorphization history. In this respect, it is meaningful to note that the as-deposited and melt-quenched $Ge_2Sb_2Te_5$ have different activation energies for crystallization [34]. The analysis of structural and electronic properties indicates that the ideal glass represents the covalent limit of the chemical bonding of $Ge_2Sb_2Te_5$ while the resonant p-bonding character prevails in the crystalline phase. The atomic and electronic structures of the melt-quenched glass lie in between these two limiting cases.

Acknowledgments

This work was supported by Samsung Electronics and the Korea Research Foundation Grant funded by the Korean Government (MOEHRD) (KRF-2008-313-C00285). The computations were carried out at the KISTI Supercomputing Center (KSC-2009-S03-0008).

References

[1] Wuttig M and Yamada N 2007 *Nat. Mater.* **6** 824
[2] Eom J H, Yoon Y G, Park C, Lee H, Im J, Suh D S, Noh J S, Khang Y and Ihm J 2006 *Phys. Rev.* B **73** 214202
[3] Kolobov A V, Fons P, Frenkel A I, Ankudinov A L, Tominaga J and Uruga T 2004 *Nat. Mater.* **3** 703
[4] Baker D A, Paesler M A, Lucovsky G, Agarwal S C and Taylor P C 2006 *Phys. Rev. Lett.* **96** 255501
[5] Jóvári P, Kaban I, Steiner J, Beuneu B, Schöps A and Webb M A 2008 *Phys. Rev.* B **77** 035202
[6] Mott N F 1967 *Adv. Phys.* **16** 49
[7] Zallen R 1983 *The Physics of Amorphous Solids* (New York: Wiley)
[8] Akola J and Jones R O 2007 *Phys. Rev.* B **76** 235201
[9] Caravati S, Bernasconi M, Kühne T D, Krack M and Parrinello M 2007 *Appl. Phys. Lett.* **91** 171906
[10] Sun Z, Zhou J, Blomqvist A, Johansson B and Ahuja R 2009 *Phys. Rev. Lett.* **102** 075504
[11] Akola J, Jones R O, Kohara S, Kimura S, Kobayashi K, Takata M, Matsunaga T, Kojima R and Yamada N 2009 *Phys. Rev.* B **80** 020201(R)
[12] Caravati S, Bernasconi M, Kühne T D, Krack M and Parrinello M 2009 *J. Phys.: Condens. Matter* **21** 255501
[13] Hegedüs J and Elliott S R 2008 *Nat. Mater.* **7** 399
[14] Xu M, Cheng Y Q, Sheng H W and Ma E 2009 *Phys. Rev. Lett.* **103** 195502
[15] Lacaita A L and Wouters D J 2008 *Phys. Status Solidi* a **205** 2281
[16] Kresse G and Hafner J 1993 *Phys. Rev.* B **47** 558
[17] Blöchl P E 1994 *Phys. Rev.* B **50** 17953
[18] Perdew J P, Burke K and Ernzerhof M 1996 *Phys. Rev. Lett.* **77** 3865
[19] Baldereschi A 1973 *Phys. Rev.* B **7** 5212
[20] Ceperley D M and Alder B J 1980 *Phys. Rev. Lett.* **45** 566
[21] Perdew J P, Ernzerhof M and Burke K 1996 *J. Chem. Phys.* **105** 9982
[22] Heyd J, Scuseria G E and Ernzerhof M 2003 *J. Chem. Phys.* **118** 8207
[23] http://www.pwscf.org
[24] Njoroge W K, Wöltgens H W and Wuttig M 2002 *J. Vac. Sci. Technol.* A **20** 230
[25] Jóvári P, Kaban I, Steiner J, Beuneu B, Schöps A and Webb A 2007 *J. Phys.: Condens. Matter* **19** 335212
[26] Chelikowsky J R and Phillips J C 1978 *Phys. Rev.* B **17** 2453
[27] Littlewood P B 1980 *J. Phys. C: Solid State Phys.* **13** 4855
[28] Ovshinsky S R 1976 *Phys. Rev. Lett.* **36** 1469
[29] Lankhorst M H R 2002 *J. Non-Cryst. Solids* **297** 210
[30] Gonze X and Lee C 1997 *Phys. Rev.* B **55** 10355
[31] Sanville E, Kenny S D, Smith R and Henkelman G 2007 *J. Comput. Chem.* **28** 899
[32] Shportko K, Kremers S, Woda M, Lence D, Robertson J and Wuttig M 2008 *Nat. Mater.* **7** 653
[33] Lencer D, Salinga M, Grabowski B, Hickel T, Neugebauer J and Wuttig M 2008 *Nat. Mater.* **7** 972
[34] Park J, Kim M R, Choi W S, Seo H and Yeon C 1999 *Japan. J. Appl. Phys.* **38** 4775